引用格式：XIE Lingli, WANG Xiaokai, HAN Xinghui, et al. Defect Detection Method for R-zone of Ribbed Components Using Distributed Laser Ultrasonics[J]. Acta Photonica Sinica, 2023, 52(2):0212002
谢玲丽,汪小凯,韩星会,等.基于分布式激光超声的带筋构件R区缺陷检测方法[J].光子学报,2023,52(2):0212002

基于分布式激光超声的带筋构件R区缺陷检测方法

谢玲丽,汪小凯,韩星会,曾研,戴殊同
(武汉理工大学 汽车工程学院 现代汽车零部件技术湖北省重点实验室,武汉 430070)

摘　要:针对带筋构件R区多类型缺陷的快速检测和精确识别等难题,提出基于分布式激光超声的带筋构件R区缺陷检测和分类识别方法。通过建立有限元模型研究了激光超声在带筋构件中的传播规律及其与R区表面裂纹、近表面气孔等缺陷的相互作用机理,进而设计制作了含典型人工缺陷的6061铝合金带筋构件试样,开展激光超声检测实验。实验获得的缺陷时域信号与B-scan特征图像及仿真结果一致,基于反射与衍射原理实现了对带筋构件R区缺陷定位与定量检测,从而验证了所提分布式激光超声检测方法的可行性,为带筋构件制造缺陷的快速检测和分类识别提供了新思路。

关键词:激光光学;分布式激光超声;多类型缺陷;带筋构件;定量检测
中图分类号:TN249　　**文献标识码**:A　　**doi**:10.3788/gzxb20235202.0212002

0 引言

带筋构件具有承载力高、重量轻等特点,普遍应用于航空航天及国防装备等领域,如航天飞机的机身整体壁板、运载火箭燃料贮箱整体壁板、导弹舱体和锥形壳体等[1]。美国生产Ti-6Al-4V钛合金整体隔框锻件用于战机装备[2];俄罗斯制造的大型整体挤压带筋壁板用于野牛登陆舰船等装备[3];我国生产了TC11、TC4钛合金带筋锻件用于波音飞机翼芯等航天装备[4]。这些带筋构件结构复杂,筋高宽比大,壁板薄[5]。带筋大型壁板制造方法通常有铣削加工、焊接成形及旋压成形等,制造过程容易产生各类型缺陷,比如在铣削过程中易出现裂纹、划痕等缺陷,焊接成形过程中焊接处易产生气孔、夹杂等缺陷,旋压成形过程中在圆角处易产生断裂、穿筋等缺陷[6]。这些缺陷会严重降低构件的承载能力和疲劳强度,影响相关装备整机的服役性能和服役安全。

目前,航空大型带筋构件无损检测技术主要有渗透检测、常规超声检测和射线检测。渗透检测主要用于检测表面裂纹、划痕等缺陷,常规超声检测用于检测内部裂纹、气孔等缺陷,射线检测用于检测内部气孔、夹杂等缺陷,这些检测方法存在接触耦合难、检测效率低、检测信息滞后等问题[7-8]。激光超声检测技术是近年发展起来的无损检测技术,具有复杂结构适应力强、缺陷灵敏度与分辨率高等特点[9],通过激光辐射材料表面激发出表面波、横波和纵波等超声波来检测材料缺陷。Lockheed Martin公司成功研制出Laser UT激光超声系统用于检测飞机机身复合材料;PEI C X等[10]建立激光声磁检测系统,通过不同位置接收到衍射横波实现缺陷定量检测;NICOLA M等[11-12]利用激光超声对涂层铁路车轴、列车车轮进行缺陷评估;中国航空制造技术研究院[13]通过激光超声对复合材料层压板开展了缺陷检测及判别研究。本文通过研究激光超声与不同类型缺陷的相互作用规律,提出带筋构件R区多类型缺陷的分布式激光超声检测方法,并开展带筋构件R区激光超声检测建模仿真和实验验证。

基金项目:国家重点研发计划(No. 2019YFB1704500),国家自然科学基金(Nos. 51875428, U21A20131),湖北省重点研发计划(No. 2020BAB144)
第一作者:谢玲丽,734116697@qq.com
通讯作者:汪小凯,wxk0919@whut.edu.cn
收稿日期:2022-07-21;**录用日期**:2022-10-11

1 带筋构件R区分布式激光超声检测方法与模型建立

1.1 激光超声理论基础

激光照射带筋构件时能量转换主要是热传导过程，将激光能量等效为固体表面热源输入，带筋构件内部热传导可以用圆柱坐标系下热传导方程来表示[14]，即

$$\rho c\frac{\partial}{\partial t}\left[T(r,z,t)\right]=\frac{1}{r}\frac{\partial}{\partial r}\left[rk\frac{\partial T(r,z,t)}{\partial r}\right]+\frac{\partial}{\partial z}\left[k\frac{\partial T(r,z,t)}{\partial z}\right] \tag{1}$$

式中，ρ为材料的密度，c为材料的比热容，$\partial T(r,z,t)$为t时刻固体的瞬时温度变化情况，r为激光半径，z为纵坐标，k为材料的热传导系数。

激光照射在带筋构件固体表面上的初始条件[15]可以描述为

$$I_0=E/(t_0\pi R_a^2) \tag{2}$$

$$-k\frac{\partial T(r,z,t)}{\partial z}\bigg|_{z=0}=I_0 g(t)f(x) \tag{3}$$

$$g(t)=\frac{t}{t_0}\exp\left(-\frac{t}{t_0}\right) \tag{4}$$

$$f(x)=\exp\left(-\frac{2(x-x_0)^2}{R_a^2}\right) \tag{5}$$

式中，I_0为入射激光功率密度，E为激光能量，t_0为激光器的上升时间，R_a为激光在x方向上的半径，$g(t)$、$f(x)$分别为激光能量在时间和空间的分布，x_0为激光中心的横坐标。

烧蚀机制下，熔化、汽化物质和等离子体产生的法向冲力作用于材料表面，激励出表面波、横波和纵波，烧蚀机制激光能量大，材料产生的热弹能量可忽略不计。弹性固体介质中的波动方程[16]可写为

$$(\lambda+\mu)\nabla\nabla\boldsymbol{U}+\mu\nabla^2\boldsymbol{U}=\rho\frac{\partial^2\boldsymbol{U}}{\partial^2 t^2} \tag{6}$$

式中，λ和μ为固体材料lame常数，$\boldsymbol{U}$为瞬态位移。

激光照射在带筋构件表面的能量可以描述为

$$P=P_0 g(t)f(x) \tag{7}$$

式中，P为构件表面吸收的总能量，P_0为入射中心的激光强度。

通过式(1)～(7)进行带筋构件激光超声检测有限元建模，研究声波在带筋构件R区传播及其与缺陷作用机理。

1.2 带筋构件分布式激光超声检测方法及模型建立

带筋构件分布式激光超声检测方法为：首先选取合适的脉冲激光器和激光接收源之间的距离w；结合带筋结构特点选取一个激发点、两个接收点，两接收点分布在带筋构件R区两侧，图1(a)为分布式激光超声

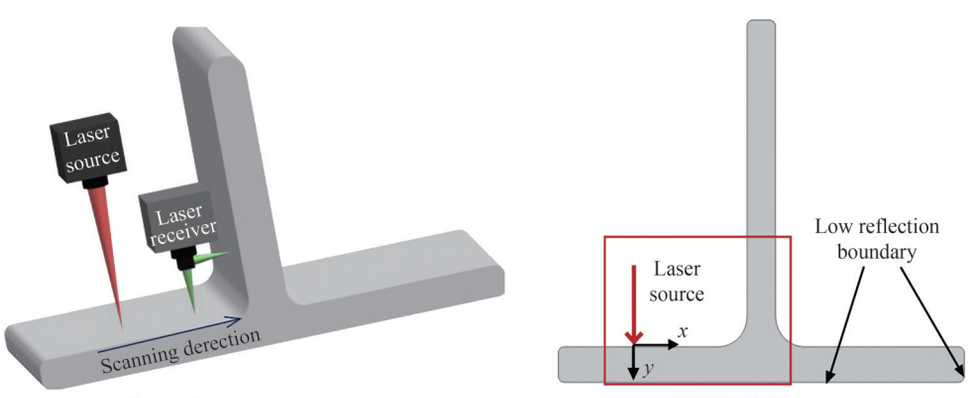

图1 分布式激光超声检测方法

Fig.1 Distributed laser ultrasonic testing method

检测示意图。分束镜调整光路，同时观察聚焦点，以确保两束检测接收光的灵敏度；控制二维扫描平台，实现对带筋构件的扫描检测。若构件存在缺陷，则声波与缺陷相互作用，最后根据两个接收点波形特征信号，实现带筋构件R区表面裂纹、气孔等典型缺陷的高效、可靠、精确检测和分类识别。

在COMSOL中建立薄壁带筋构件激光超声检测有限元模型，以激发激光为原点建立平面直角坐标系，模型见图1(b)。其中，激发激光脉冲能量为50 mJ，光源半径为0.2 mm，脉宽为10 ns，为保证数值模型的稳定，模型设置时间步长为2 ns；为了保证仿真效率和结果正确，选用三角形网格，R区处网格最大单元为0.06 mm，其他区域最大单元为0.08 mm。带筋构件材料为铝合金，计算时所需参数如表1所示。带筋构件的高为70 mm，壁板壁厚为7 mm，高筋厚度为6 mm。激发点坐标为(0，0)，设置裂纹缺陷深度为1 mm，宽为0.1 mm；设置气孔缺陷直径为1.2 mm，与接收点1夹角均为43°。其中，激光激发与接收点1的距离固定为w=13.5 mm，接收点1位于构件圆角与壁板衔接处，坐标为(13.5，0)；接收点2位于沿圆角向上与高筋衔接处，坐标为(19.7，−6.2)。

表1　带筋构件材料参数

Table 1　Material parameters of ribbed component

Material properties	Constant pressure heat capacity/ ($J\cdot kg^{-1}\cdot K^{-1}$)	Density/ ($kg\cdot m^{-3}$)	Thermal conductivity/ ($W\cdot m^{-1}\cdot K^{-1}$)	Elastic modulus/Gpa	Poisson ratio
Value	896	2 850	154	68	0.34

1.3　仿真结果分析

由仿真得到图2，分别给出在4 μs、8 μs、10 μs时刻声波传播情况，其中sP表示掠面纵波，L波表示纵波，S波表示横波，R波表示表面波，RR波表示反射表面波，RS波表示表面波转横波，SC波表示横波转爬波，

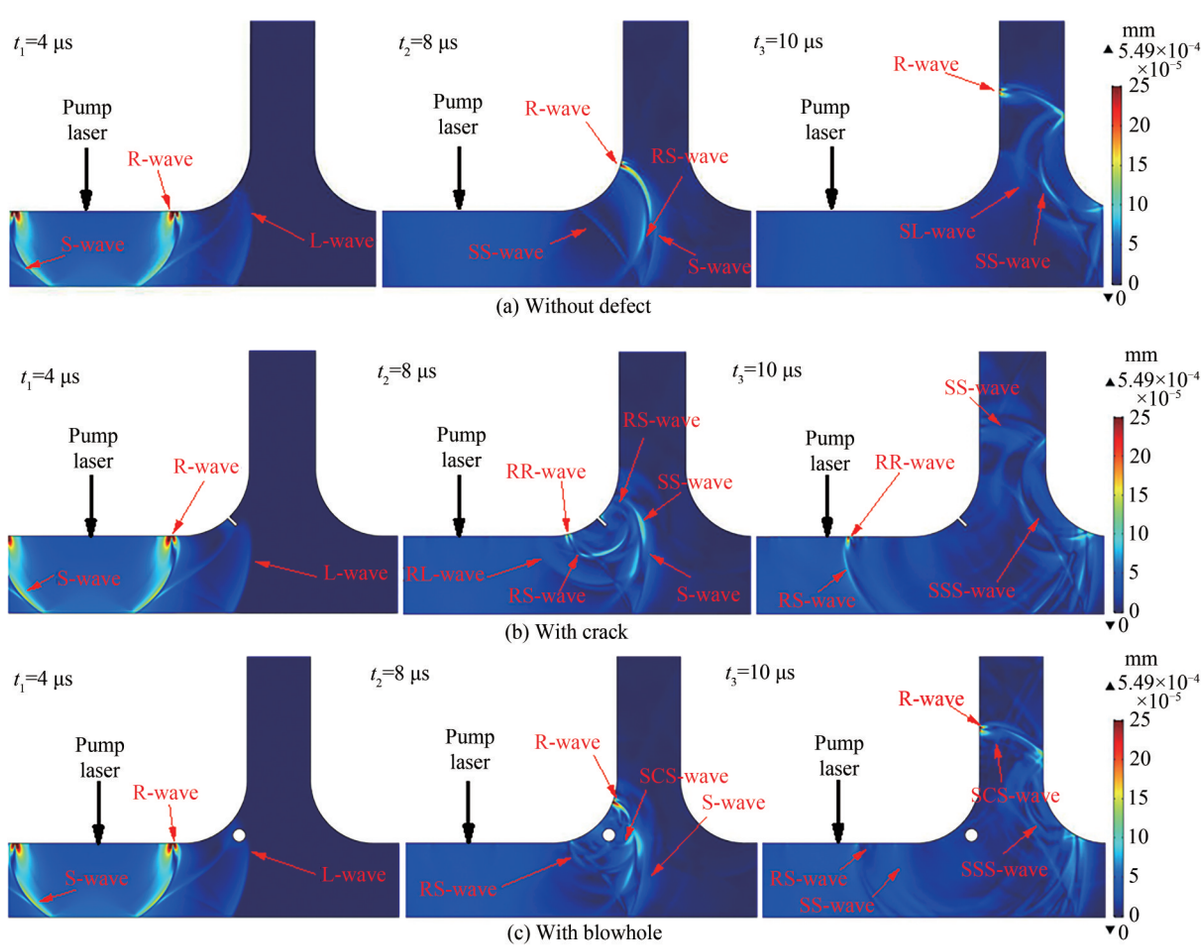

图2　激光超声有限元仿真的声波图

Fig. 2　The sonic diagram of laser ultrasonic finite element simulation

SCS波表示横波转爬波再转横波，RL波表示表面波转纵波，SS波表示横波转横波，SL波表示横波转纵波，SSS波表示横波转横波转横波。

图2(a)所示，带筋构件R区无缺陷时，S波向右传播至右侧圆角处发生反射，产生SS波、SL波沿圆角两侧传播；R波从筋板表面沿圆角向上传播。图2(b)所示，R区存在表面裂纹时，S波传播至裂纹处，作用产生SS波，与高筋右半边圆角作用产生SS波、SR波；R波与裂纹反射产生RR波沿原路传播，部分R波沿裂纹表面传播后发生衍射，产生RS波，与无缺陷对比，RS波信号微弱。图2(c)所示，R区存在近表面气孔时，首先部分S波传播至气孔并沿表面传播产生SC波，SC波沿气孔表面传播一段距离后离开气孔形成SCS波，R波与气孔衍射产生RS波沿原路传播，部分R波沿气孔与R区表面空隙向上传播，与无缺陷对比，接收到R波信号较弱。根据上述分析表明R区存在不同缺陷时，声波与缺陷作用机理不同，可提取不同缺陷的特征信号。

图3为不同缺陷检测原理图，根据特征波形传播路径，接收点1接收的反射缺陷回波RR波、RS波，接收点2接收的衍射波RS波、RL波、SCS波，可以对带筋构件R区缺陷分类识别。纵波、表面波及横波速度v_{L}、v_{R}、v_{S}的计算公式为

$$\begin{cases} v_{\mathrm{L}} = w/t_{\mathrm{sP}} \\ v_{\mathrm{R}} = w/t_{\mathrm{R}} \\ v_{\mathrm{S}} = w/t_{\mathrm{S}} \end{cases} \tag{8}$$

式中，t_{sP}、t_{R}、t_{S}为掠面纵波、表面波及横波到达时间。因sP波和L波、SCS波和S波声速相近，故假设$v_{\mathrm{sP}}=v_{\mathrm{L}}$、$v_{\mathrm{SCS}}=v_{\mathrm{S}}$。裂纹缺陷两接收点测得的表面波和反射表面波波形到达时间t_{R}、t_{RR}与筋部几何尺寸，以及声程L_{OD}、L_{BD}的关系为

$$\begin{cases} L_{BD} = r\cos\theta_1 \\ L_{OD} = r\sin\theta_1 \\ t_{\mathrm{RR}} = (w + 2r\theta_1)/v_{\mathrm{R}} \\ t_{\mathrm{RS}} = (w + r\theta_1 + h)/v_{\mathrm{R}} + \sqrt{{L_{BD}}^2 + (r + h - L_{OD})^2}/v_{\mathrm{S}} \end{cases} \tag{9}$$

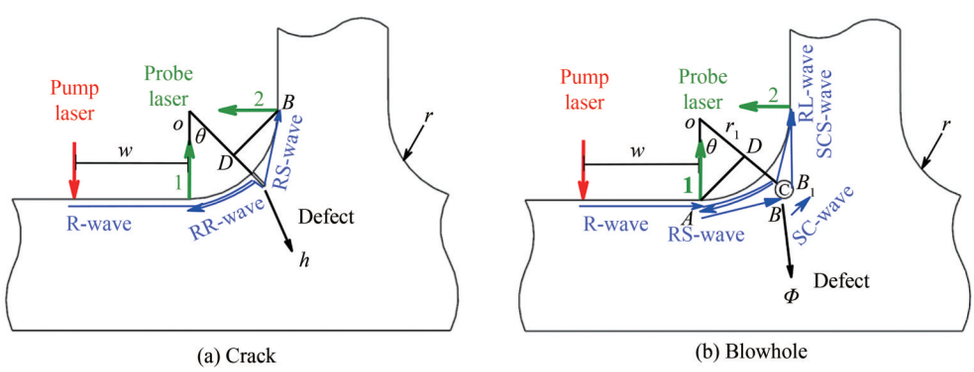

图3 不同缺陷检测原理

Fig.3 Schematic diagram of different defect detection

气孔缺陷两接收点测得的表面波转横波、表面波转纵波及横波转爬波再转横波波形到达时间t_{RS}、t_{RL}、t_{SCS}与筋部几何尺寸、声程L_{AD}、L_{CD}、L_{AB}、L_{BB_1}的关系为

$$\begin{cases} L_{AD} = r\sin\theta_2 \\ L_{CD} = r_1 - r\cos\theta \\ L_{AB} = \sqrt{{L_{AD}}^2 + {L_{CD}}^2 - (\phi/2)^2} \\ L_{BB_1} = 2\times\left(\pi - \arctan\dfrac{L_{AD}}{L_{CD}} - \arctan\dfrac{L_{AB}}{\phi/2}\right)\times(\phi/2) \\ t_{\mathrm{RS}} = (w + r\theta_2)/v_{\mathrm{R}} + r\theta_2/v_{\mathrm{S}} \\ t_{\mathrm{RL}} = (w + r\theta_2)/v_{\mathrm{R}} + \sqrt{{L_{AD}}^2 + (L_{CD} - \phi/2)^2}/v_{\mathrm{L}} \\ t_{\mathrm{SCS}} = (w + 2L_{AB})/v_{\mathrm{S}} + L_{BB_1}/v_{\mathrm{S}} \end{cases} \tag{10}$$

由此可计算裂纹、气孔缺陷在圆角处夹角θ_1、θ_2、裂纹深度h、气孔直径ϕ和气孔中心到圆角圆心的距离r_1，其中t_{sP}为掠面纵波到达时间，r为圆角半径。

2 带筋构件R区激光超声检测系统设计与实验验证

2.1 带筋构件分布式激光超声检测系统

对构件近表面缺陷进行分布式激光超声检测的系统如图4所示。激光激发源为Nd:YAG激发器，能产生波长为1 064 nm，脉宽为10 ns的脉冲激光，脉冲能量和重复频率通过控制器设置为50 mJ和50 Hz，由此激发激光。激光接收源是QUARTET接收器，能产生波长为532 nm的连续激光，采用立方体分束镜将检测激光分成两束分别分布在不同位置进行两处信号接收。在待检带筋构件上标识激光激发和检测激光的位置与仿真时一致，将带筋构件放置在二维移动平台上，调整激光激发和检测激光光束对准标识位置，通过软件控制，实现移动扫查。

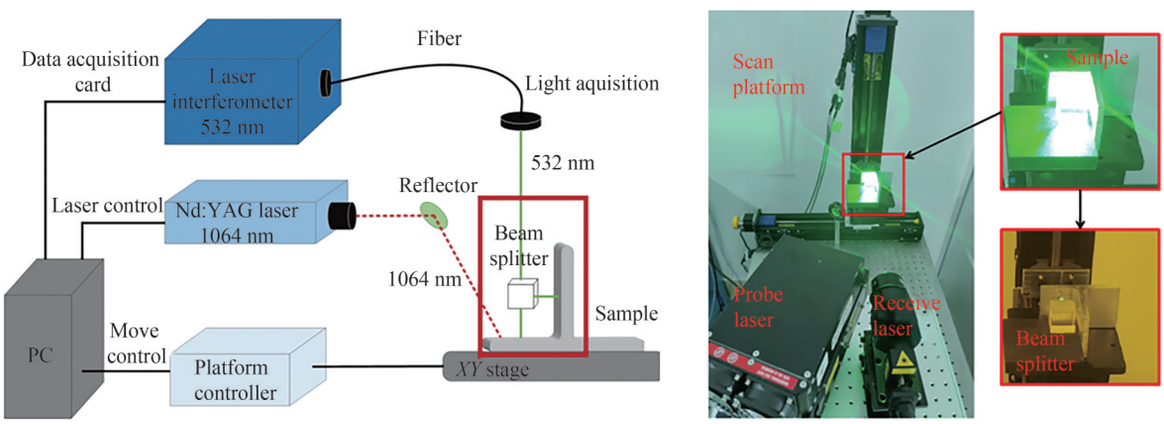

图4 激光超声检测系统

Fig.4 Laser ultrasonic detect system

为了验证分布式激光超声综合检测方法的可行性，开展了针对裂纹、气孔等缺陷的激光超声检测实验。采用6061铝合金带筋构件，带筋试块壁板壁厚h_1为7 mm，高筋厚度h_2为6 mm，圆角半径r为6.2 mm，图5为加工缺陷在带筋构件R区位置示意图及实物图，分别以槽、横通孔模拟表面裂纹和近表面气孔，其中槽深度h为1.15 mm，横通孔直径为Φ1.2 mm，横通孔中心到圆角圆心的距离r_1为7.8 mm，且在圆角处夹角均为43°。

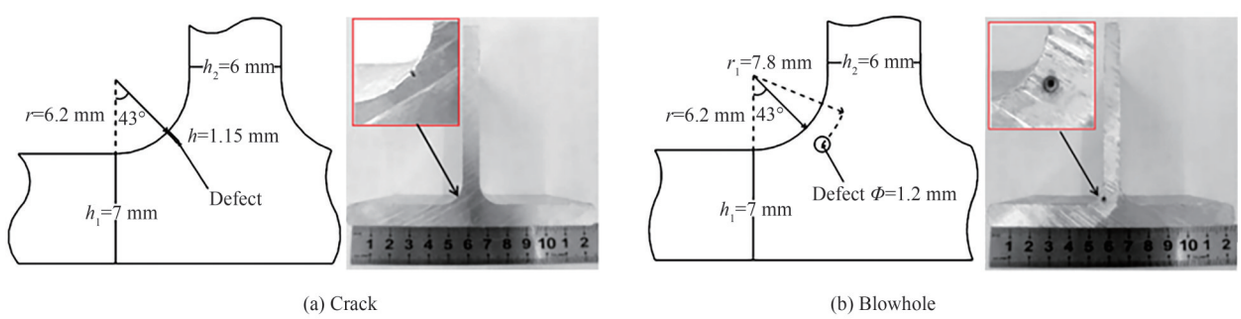

图5 加工缺陷尺寸示意图

Fig.5 Schematic diagram of the size of the processing defect

以检测第一个试块的缺陷为例，采用遮光镜遮挡分束镜一个方向的检测光，按图1检测带筋构件R区的扫查方向，通过控制二维移动平台，进行一次扫查，在扫查过程中每个扫查点采集50次信号，取其平均再记录，从而提高信噪比，获得接收点1的时域波形图及B-scan图像；随后将遮光镜遮住分束镜另一个方向的检测光，进行二次扫查，获得接收点2的时域波形图以及B-scan图像，其中扫查步长为0.02 mm，扫查距离为3.5 mm。

2.2 实验结果分析

图6、7为带筋构件R区表面裂纹、近表面气孔在接收点1和2处的仿真-实验时域波形图，可以看出仿真与实验时域波形在幅值最大值和信号特征高度一致，证明实验的正确性。图8、9分别为对应的实验B-scan图像。由图6(a)、图7(a)可获得裂纹缺陷、气孔缺陷实验的横波平均到达时间 t_R=4.65 μs，根据式(8)计算得到横波的传播速度，v_S=2 904 m/s，已知材料属性计算横波理论速度 $v_S=\sqrt{\dfrac{E}{2\rho(1+\sigma)}}$=2 980 m/s，其中理论与实验测得横波速度相对误差为2.5%，再次验证了实验的正确性。

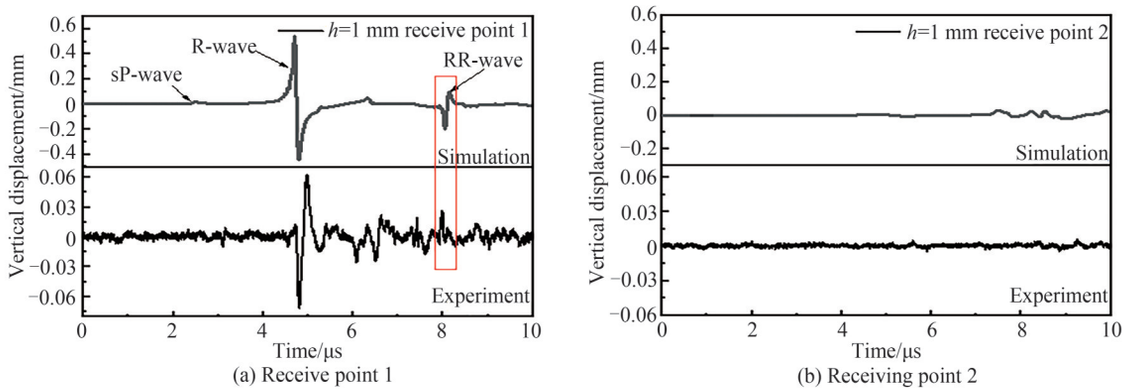

图6 裂纹缺陷接收点时域波形

Fig.6 The time domain waveform of receiving point for crack defect

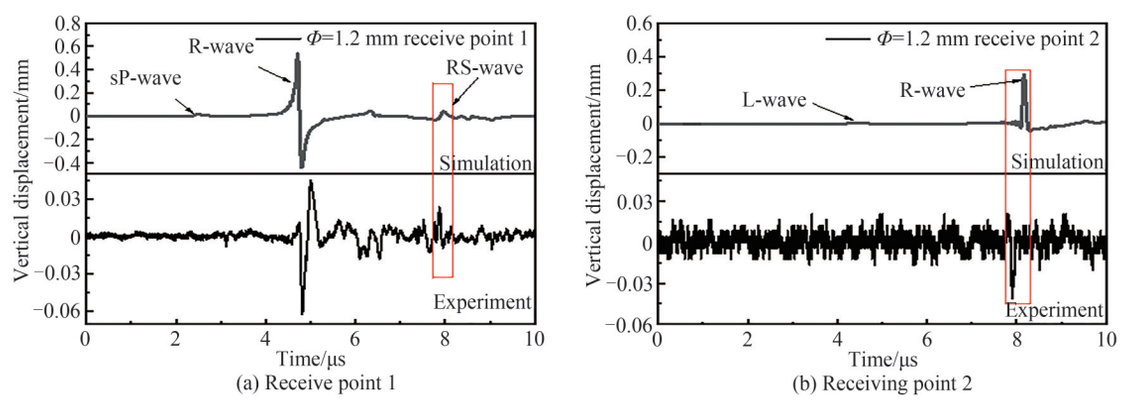

图7 气孔缺陷接收点时域波形

Fig.7 The time domain waveform of receiving point for blowhole defect

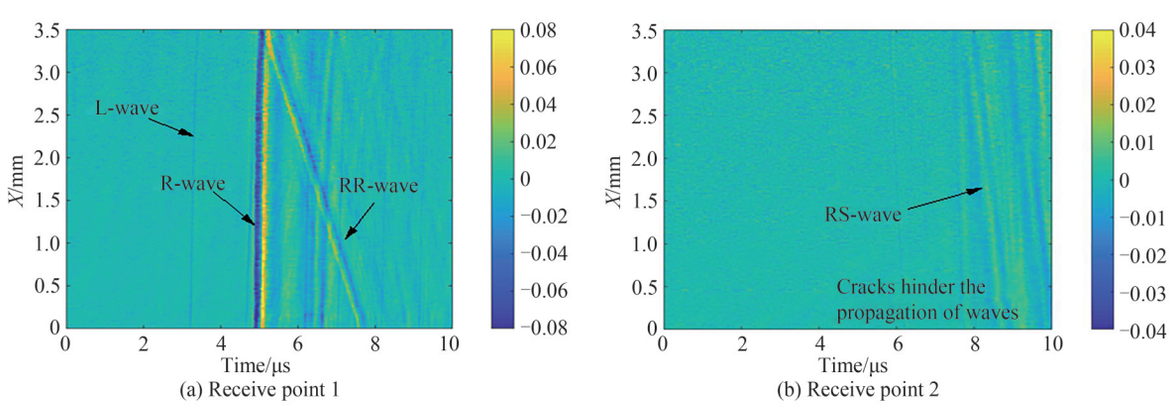

图8 实验所得裂纹缺陷B-scan图像

Fig.8 Experimental crack defect B-scan

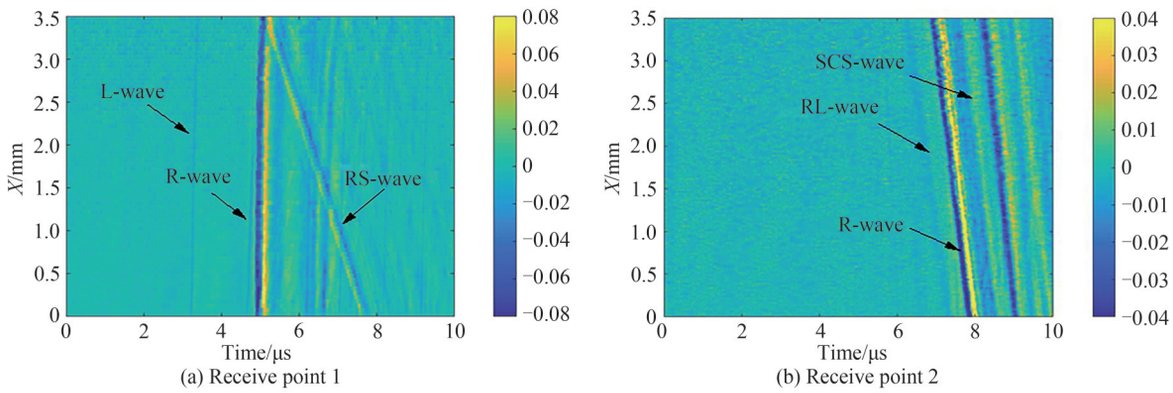

图9　实验所得气孔缺陷B-scan图像

Fig.9　Experimental blowhole defect B-scan

由图6、8可知对带有裂纹缺陷构件检测时，接收点1能明显接收到sP波、R波和RR波，接收点2能接收到RS波，裂纹阻碍R波的传播，无法接收到高幅值R波。由图7、9可知对带有气孔缺陷构件检测时，接收点1能明显接收到sP波、R波和RS波，接收点2也能接收到RL波、高幅值R波和SCS波。其中图8、9中RR波与RS波的到达时间随着扫查距离的变化而变化，当接收点1位于裂纹或气孔缺陷的正上方时，R波与RR波、RS波到达时间相同，在B-scan图像中呈相交状。综上，仿真与实验的特征信号高度一致，可实现带筋构件R区表面裂纹、近表面气孔等典型缺陷的分类识别，验证了分布式激光超声综合检测方法的可行性。

2.3　缺陷定位与定量计算

根据实验B-scan图像中各接收点特征波形的到达时间、声速及声程公式(9)、(10)，即可求出裂纹、气孔缺陷在圆角处夹角θ_1、θ_2、裂纹深度h、气孔直径ϕ和气孔中心到圆角圆心的距离r_1。通过实验获得表面波与掠面纵波平均到达时间t_R=4.73 μs，t_{sP}=2.5 μs，由式(8)计算得v_R=2 856 m/s，v_{sP}=5 400 m/s。重复两组实验，并取扫查距离x=0 mm为测量点，可得到三组扫查B-scan图像，其中各模式声波到达时间如表2所示。

表2　各模式声波到达时间

Table 2　Wave arrival time for each mode

Measurement point	Crack		Blowhole		
	t_{RR}/μs	t_{RS1}/μs	t_{RS2}/μs	t_{RL}/μs	t_{SCS}/μs
1	7.90	8.72	7.81	7.16	8.52
2	7.94	8.67	7.83	7.19	8.58
3	7.92	8.71	7.84	7.20	8.60

根据式(9)、(10)对各参数进行计算得到缺陷位置与尺寸，并计算绝对误差和相对误差，结果如表3所示，其中θ进行弧度转换$\theta=\theta\cdot180°/\pi$。实验结果表明：分布式激光超声综合检测方法可实现带筋构件R区表面裂纹、近表面气孔等典型缺陷的定位定量，裂纹深度、相对圆角位置，气孔直径、相对圆角位置均可检测得出，其中裂纹定位相对误差为3.2%，裂纹定量相对误差为7.8%；气孔定位相对误差(包括气孔相对圆角角

表3　缺陷位置与尺寸

Table 3　Defect location and size

Parameter	Design value	Measurement point			Measure absolute error	Relative error
		Point 1	Point 2	Point 3		
$\theta_1\cdot\frac{180}{\pi}$/(°)	43	41.90	42.40	42.14	0.85	3.2%
h/mm	1.15	1.21	1.19	1.23	0.09	7.8%
$\theta_2\cdot\frac{180}{\pi}$/(°)	43	41.02	41.28	41.42	1.76	4.1%
ϕ/mm	1.20	1.36	1.32	1.33	0.14	11.7%
r_1/mm	7.80	7.82	7.90	7.92	0.08	1.1%

度和气孔到圆角圆心距离误差)为4.1%、1.1%,气孔定量相对误差为11.7%。另外,气孔定量相对误差过大的问题,一方面是因为在计算定量误差时,只能将v_{SCS}近似为v_S,但实际上二者略有不同;另一方面是因为圆角内部凸面使声波发散,对衍射波信号接收有一定影响。

3 结论

本文揭示了激光超声在带筋构件中的传播规律及其与R区表面裂纹、近表面气孔等典型缺陷的相互作用机理,提出了基于分布式激光超声的带筋构件R区缺陷检测方法。

分布式激光超声检测实验结果表明,各类型缺陷的时域波形特征与仿真一致,进一步获得了表面裂纹、气孔等典型缺陷的B-scan图像,验证了所提检测方法的可行性。该方法实现了带筋构件R区表面裂纹、内部气孔等典型缺陷的分类识别与定位定量,定位相对误差在≤5%,定量相对误差≤12%,可为带筋构件制造缺陷的快速可靠检测提供新思路。

参考文献

[1] PENG Lu. Research on envelope forming method for thin-walled cylindrical components with high ribs[D]. Wuhan: Wuhan University of Technology, 2020.
彭露. 薄壁高筋筒形构件包络辗压成形方法研究[D]. 武汉:武汉理工大学, 2020.

[2] QI Han. Research on rules of rib cavity fill and defects of web-rib parts[D]. Harbin: Harbin Institute of Technology, 2010.
齐晗. 筋板件筋部充填机理及缺陷研究[D]. 哈尔滨:哈尔滨工业大学, 2010.

[3] LI Qianyun, HU Yong, WANG Chen, et al. Research of precise manufacturing technology for large thin wall panel with high ribs made of high strength aluminum alloy[J]. Astronautical Systems Engineering Technology, 2021, 5(1): 19-26.
李倩云, 胡勇, 王辰, 等. 高强铝合金薄壁高筋大型壁板精确成形制造技术研究[J]. 宇航总体技术, 2021, 5(1): 19-26.

[4] MENG Qingtong, PANG Kechang, ZHOU Jianhua. Isothermal forging technology of titanium alloy casing forging[J]. The Chinese Journal of Nonferrous Metals, 2010, 20(S1): 862-864.
孟庆通,庞克昌,周建华. 钛合金机匣精锻件等温锻造技术[J]. 中国有色金属学报, 2010, 20(S1): 862-864.

[5] YE Jingshen, ZHANG Baohong, YU Jianmin, et al. Research progress of component with rib forming technology[J]. China Metalforming Equipment & Manufacturing Technology, 2015, 50(2): 7-10.
叶景申, 张宝红, 于建民, 等. 筋板类构件成形技术研究进展[J]. 锻压装备与制造技术, 2015, 50(2): 7-10.

[6] ZHONG Xinyue, DU Shangjun, LI Zhiyuan, et al. Defect control method and application of spinning forming[J]. Journal of Netshape Forming Engineering, 2020, 12(6): 169-174.
仲昕岳, 杜尚军, 李志远, 等. 旋压成形过程缺陷控制方法及应用[J]. 精密成形工程, 2020, 12(6): 169-174.

[7] DU Dong, CAI Guorui, TIAN Yuan, et al. Automatic inspection of weld defects with X-ray real time imaging[J]. Lecture Notes in Control and Information Science, 2007, 362: 359-366.

[8] QIU Jinhao, ZHANG Chao, JI Hongli, et al. Non-destructive testing for aerospace composite structures using laser ultrasonic technique[J]. Aeronautical Manufacturing Technology, 2020, 63(19): 14-23.
裘进浩, 张超, 季宏丽, 等. 面向航空复合材料结构的激光超声无损检测技术[J]. 航空制造技术, 2020, 63(19): 14-23.

[9] LI Chunhui, LI Sinan, GUAN Guangying, et al. A comparison of laser ultrasonic measurements and finite element simulations for evaluating the elastic properties of tissue mimicking phantoms[J]. Optics & Laser Technology, 2012, 44(4): 866-871.

[10] PEI C X, FUKUCHI T, ZHU H T, et al. A study of internal defect testing with the laser-EMAT ultrasonic method[J]. IEEE Transactions on Ultrasonics, Ferroelectrics and Frequency Control, 2012, 59(12): 2702-2708.

[11] NICOLA M, GABRIELLA E, DONATELLA C, et al. Laser ultrasonics for defect evaluation on coated railway axles[J]. NDT and E International, 2020, 116: 102321.

[12] NICOLA M, GABRIELLA E, DONATELLA C, et al. Laser ultrasonics inspection for defect evaluation on train wheel[J]. NDT and E International, 2019, 107: 102145.

[13] LIU Songping, GUO Enming, LIU Feifei, et al. Evaluation of defects in carbon fiber-reinforced composites by laser ultrasonic technique[J]. Nondestructive Testing, 2007, 29(7): 396-401.
刘松平, 郭恩明, 刘菲菲, 等. 激光超声检测碳纤维增强树脂基复合材料的缺陷评估技术研究[J]. 无损检测, 2007, 29(7): 396-401.

[14] CHEN C, ZHANG X Y. Research on laser ultrasonic surface defect identification based on a support vector machine[J]. Science Progress, 2021, 104(4): 1-17.

[15] ZHANG Kuanshuang, LI Shicheng, ZHOU Zhenggan. Detection of disbonds in multi-layer bonded structures using the laser ultrasonic pulse-echo mode[J]. Ultrasonics, 2018, 94: 411-418.

[16] QIN Feng, WU Yaojin, GUO Hualing, et al. Laser ultrasonic nondestructive testing based on nonlinear ultrasonic coefficient[J]. Russian Journal of Nondestructive Testing, 2020, 56(3): 209-221.

Defect Detection Method for R-zone of Ribbed Components Using Distributed Laser Ultrasonics

XIE Lingli, WANG Xiaokai, HAN Xinghui, ZENG Yan, DAI Shutong

(*School of Automotive Engineering, Hubei Key Laboratory of Advanced Technology of Automotive Components, Wuhan University of Technology, Wuhan* 430070, *China*)

Abstract: On account of the characteristics of high bearing capacity and lightweight, the ribbed components are widely applied to aerospace and national defense equipment, such as the overall wall of the fuselage of the space shuttle, the overall wall of the fuel tank of the launch vehicle, the missile cabin, and the conical shell body. The manufacturing methods of large-scale ribbed components usually include milling, welding, and spinning. Therefore, various types of defects are also brought during the manufacturing process, such as cracks and scratches. During the milling forming process, pores and inclusions in the welding, fractures, and rib penetration at the rounded corners during the spinning, which will seriously reduce the bearing capacity and fatigue strength of the components thus affecting the service performance and safety of related equipment.

To solve the problems of rapid detection and precise identification of multi-type defects in the R-zone of ribbed components, this paper innovatively proposed a method for the detection, classification, and identification of defects in the R-zone of ribbed components based on distributed laser ultrasonics. Combining the characteristic signals of multiple detection receiving points, this method realizes the classification, identification with quantitative detection of the defects in the R-zone of the ribbed component; and it was carried out that the modeling simulation and experimental verification of the laser ultrasonic detection of the R-zone of the ribbed components.

Firstly, finite element models were established to study the propagation law of laser ultrasound in ribbed components and the interaction mechanism between laser ultrasound and defects such as surface cracks and near-surface blowholes in the R-zone; then based on the above-mentioned propagation law and the structural characteristics of the ribbed member, two detection receiving points were set at both sides of the R-zone of the ribbed component. According to the characteristic waveform propagation path, the reflected defect echo RR and RS wave received at the receiving point 1, the diffracted wave RL, RS and SCS wave received at the receiving point 2 could classify and identify the defects in the R-zone of ribbed components based on the reflection and diffraction principle, and the quantitative calculation model of defect location was established through the sound path, sound velocity and the geometric size of the rib. To sum up, the distributed receiving can realize the rapid detection, classification, recognition, positioning, and quantitative detection of defects in the R-zone of ribbed components.

Then, 6061 aluminum alloy ribbed component samples were designed and manufactured with typical artificial defects (the angle between crack and fillet is 43°, the crack depth is 1.15 mm, and the angle between blowhole and fillet is 43°, the distance between the blowhole center and the center of the rounded corner is 7.80 mm, the blowhole diameter is 1.20 mm) for distributed laser ultrasonic testing experiment, and obtained the time domain waveforms of two receiving points. When testing the component with crack defect, the receiving point 1 can receive SP-wave, R-wave and RR-wave, and receiving point 2 can receive RS-wave. But it cannot receive a high amplitude R-wave because of the crack hindering the propagation of the R-wave. When detecting the component with porosity defect, receiving point 1 can obviously receive sP-wave, R-wave and RS-wave, and receiving point 2 can also receive RL-wave, SCS-wave and high amplitude R-wave, which was consistent with the simulation results, thus verifying the feasibility of distributed laser ultrasonic testing method.

At the same time, the B-scan images with different defects were obtained through experiments, then the experiment was repeated to get three groups of data in total. The arrival time of characteristic waveforms of different defects was obtained from groups of data taken from the scan position $x=0$ mm in

the three B-scan images. The positioning angle of two defects, the crack depth, the distance between the blowhole center and the center of the rounded corner, and blowhole diameter were obtained by the positioning quantitative calculation model, and the positioning quantitative calculation of the three measurement points was calculated on average. The relative error of crack positioning and crack quantification was 3.2% and 7.8%, respectively, and the relative error of blowhole positioning (including the relative angle of the blowhole and the distance from the blowhole to the center of the fillet) was 4.1% and 1.1%, and the relative error of blowhole quantification was 11.7%. Thus, the positioning and quantitative detection of defects in R-zone of ribbed components were realized. In addition, the relative error of blowhole quantification was too large for two reasons. On the one hand, it was because the speed of SCS-wave could only be approximated as the speed of S-wave when calculating the quantitative error, but in fact the two were slightly different, on the other hand, because the inner convex surface of the rounded corners made the sound waves diverge, which had a certain influence on the reception of the diffracted wave signals.

In conclusion, this study can provide a new idea for rapid detection and classification of manufacturing defects of ribbed components.

Key words: Laser optics; Distributed laser ultrasound; Different types of defects; Ribbed component; Quantitative detection

OCIS Codes: 120.4290; 140.3460; 110.7170

Foundation item: National Key Research and Development Program (No.2019YFB1704500), National Natural Science Foundation of China (Nos. 51875428, U21A20131), Hubei Provincial Key Research and Development Program (No.2020BAB144)